NJC

New Journal of Chemistry

A journal for new directions in chemistry

Accepted Manuscript

This article can be cited before page numbers have been issued, to do this please use: M. Devi, B. Das, M. H. Barbhuiya, B. Bhuyan, S. S. Dhar and S. Vadivel, *New J. Chem.*, 2019, DOI: 10.1039/C9NJ02904D.

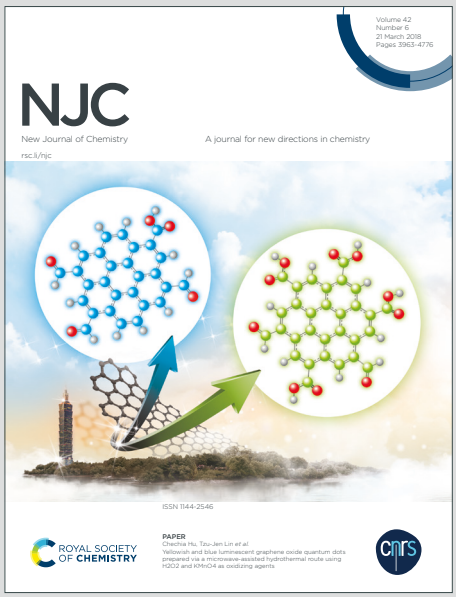

View Article Online
DOI: 10.1039/C9NJ02904D

ARTICLE

Fabrication of nanostructured NiO/WO_3 with graphitic carbon nitride for visible light driven photocatalytic hydroxylation of benzene and metronidazole degradation

Received 00th January 20xx,
Accepted 00th January 20xx

DOI: 10.1039/x0xx00000x

Meghali Devi,[a] Bishal Das,[a] Monjur Hassan Barbhuiya,[a] Bishal Bhuyan,[a] Siddhartha Sankar Dhar*[a] and Sethumathavan Vadivel[b]

In the present study we report a novel nanocatalyst prepared by the modification of g-C_3N_4 nanosheets with NiO/WO_3 nanohybrid via simple ultra-sonication method. A novel method was employed for the synthesis of NiO/WO_3 nanohybrid. The photocatalytic efficiency of the catalysts were explored in C-H activation and degradation of a pharmaceutical waste namely metronidazole. The photocatalyst recorded a rapid and highly selective conversion of benzene to phenol under irradiation by LED bulb. Degradation of metronidazole was carried out both in presence of sunlight and LED light and monitored with UV-VIS spectroscopy. It was observed that the degradation process was more efficient under solar light irradiatiion, where it recorded complete degradation in 90 minutes with a rate constant of 0.0165 min^{-1}. The modified photocatalyst showed much higher efficiency compared to individual components of g-C_3N_4 and nanostructured NiO/WO_3. The structural features of the photocatalyst were thoroughly investigated using powder XRD, SEM, TEM, XPS, UV-DRS, PL and BET analysis. This enhanced efficiency is attributed to larger surface area, lower band gap and delayed recombination of photogenarated charge carriers in the heterojunction. The critical involvement of photoactive radicals in the degradation process was thoroughly investigated by trapping experiments using photoluminescence spectroscopy.

A Introduction

Selective C-H bond functionalization has been one of the most dynamic research fields in basic studies of inert C-H bond and the potential industrial applications in petrochemicals, pharmaceuticals, agrochemicals and plastics Phenol is the key precursor in synthesis of numerous commercially important commodities like phenol resins, caprolactam, bisphenol-A etc. However, the industrial three step cumene process suffers from major drawbacks like low selectivity of phenol, polluting and formation of explosive intermediate and over-oxidized products.[1] Hence sustainable yet economical catalytic oxidation of benzene to phenol using green oxidants like molecular oxygen or hydrogen peroxide has always been a research goal. Transition metals mainly Pd, Pt, Au and Ag catalysts have been proved to be very effective in C-H activation reactions.[1-4] But to eliminate the serious drawback of being expensive and thus to attain potential high scale industrial production these catalysis processes are intended to replace with more economic and earth abundant first row transition metals. Co(III) complex have shown more efficiency over corresponding Rh complex in visible light mediated hydroxylation of benzene with O_2 as oxidant.[5] Vanadium as different catalyst, V_xO@C, VO(acac), $VOPO_4.2H_2O$, $Au/Ti_{0.98}V_{0.02}O_2$ etc. have also been reported for this transformation.[3, 6-10] Mixed metal chalcogens such as $CdS/KTa_{0.75}Nb_{0.25}O_3$, C-$KNbO_3$, MoS_2/C-$KNbO_3$ have shown attractive photocatalytic properties in the field of H_2 generation. Again $AgNbO_3$/g-C_3N_4, $KTa_{0.75}Nb_{0.25}O_3$/g-C_3N_4, $KNbO_3$/g-$C_3N_4$and boron doped g-C_3N_4have also shown high activity for photocatalytic H_2 generation.[11] Nickel has been an attractive metal for various C-H activation due to its low cost and attractive reaction profile. Efficient C-H activation of aldehydes, amines, olefins, arenes using different Ni salts and organometallic Ni(II)complexes have been described.[12,13] Though these homogeneous catalysts offer satisfactory yield and chemoselectivity under comparatively mild conditions, these catalysts are tedious and expensive to separate from the reaction mixture, thus immobilization over porous support is encouraged for effective and easier recycling. Effectively mixed n-type semiconductors ZnO, WO_3, $BiVO_4$ etc. with p-type semiconductors NiO, CuO, Cu_2O etc have found enormous applications in various fields in photo electrochemistry and photocatalysis including optical fiber, gas and humidity sensor and catalytic reactions. NiO has been extensively used in catalysts, electrochromic films, battery cathodes solar cells and magnetic materials. But its band gap impedes its direct uses in photocatalytic chemical transformations. Hence modification of NiO with an n-type semiconductor WO_3 tend to enhance its photocatalytic efficiency. Flake like NiO/WO_3 heterojunction have been established as photocathode for photoelectrochemical water splitting reaction.[14] A solid state

[a] Department of Chemistry, National Institute of Technology, Silchar, Cachar, 788010, Assam, India, E-mail: ssd_iitg@hotmail.com.
[b] Department of Chemistry, PSG College of Technology, Peelamedu, Coimbatore, 641004, Tamil Nadu, India.
Electronic Supplementary Information (ESI) available: [details of any supplementary information available should be included here].

View Article Online DOI: 10.1039/C9NJ03904D

electrochromic device consisting of WO_3 layer as main electrochromic layer, NiO layer as counter electrchromic layer and Li^+ as conductor layer over ITO glass substrate have reported for competent modulation of optical transmittance. This infers potential application in smart windows.[15] Ink-jet printed nanostructured thin film of NiO/WO_3 have shown strong adhesion with ITO glass substrate, larger optical modulation and higher coloration efficiency.[16] A high frequency electrochromic cell consisting of $WO_3/LiNbO_3/NiO$ have also been reported for tunable dielectric characteristics.[17] Another fascinating application of NiO/WO_3 heterojunction in the area of gas sensing have observed due to its high surface area and small grain size.[18] Similar compound $NiWO_4$ and its various modification has found various applications in electro chemistry, solar cells, fuel cells, photocatalytic dye degradation and catalytic organic reactions.[19] Though NiO/WO_3 have shown enormous potential in areas of sensing and photoelectrochemistry, its photocatalytic properties for organic transformations are very less explored.

The presence of pharmaceutical wastes in soil and water bodies has become a severe environmental concern as inadequately treated wastewater from sewage plants has resulted a series of serious threats including antibiotic resistant bacteria, toxicity towards aquatic life which eventually risk human health. Due to their complicated structures conventional methods of wastewater treatment like ultrasound degradation, coagulation floatation, surface adsorption etc. suffers from shortcomings of high energy consumption, production of secondary pollutants and slow degradation rate etc. Necessity of UV light for reaction initiation and high implementation cost limit the use of advanced oxidation processes (AOPs) in industrial level.[20] Recently a number of piezoelectric materials have also been reported for degradation of various antibiotics.[21,34] Metronidazole (MZ) is a very widely used, low cost, broad spectrum antimicrobial agent for various abdominal, dermatological, gynecological and respiratory infections. It is being produced in large amounts and eventually a substantial amount goes into the environment through sewage water. These leads research in the field of cost effective catalytic degradation of metronidazole using renewable energy. Various catalyst involving transition and non-transition elements have being employed for effective degradation of metronidazole. $ZnGeO_4$ hollow spheres and nanostructured Bi_4VO_8Cl are successfully employed for this process using UV lamp as source of energy.[22] Interesting degradation processes have been reported using silver doped TiO_2, CdS and ZnS nanoparticles in photoreactor involving high pressure mercury vapor lamp.[23] Again Ag doped TiO_2 hollow spheres, $CaInS_4/TiO_2$ and Fe/Si co-doped TiO_2 have been reported to show high activity towards degradation of metronidazole upon in presence of UV lamp.[21,24] Balsam pear shaped $BiVO_4/BiPO_4$ nanocomposites effectually degrades metronidazole and rhodamine-B dye upon irradiation with 500W Xenon lamp.[25] Several zinc based photocatalysts viz, ZnO, $ZnSnO_3$, $ZnSnO_4$ and $ZnIn_2S_4/Bi_2WO_6$ have also shown efficiency towards photocatalytic metronidazole degradation using energy in the ultra violet region.[26] Here catalysts involving Ag are highly expensive and cannot be practically employed in large scale wastewater treatment. Again by far most of the catalysts uses energy consuming UV lamps which also hinders their practical application.

The recent years have witnessed increase in application of carbonaceous materials like graphene, graphene oxide, graphitic nitrides, carbon nanotubes and activated carbon in numerous areas of catalysis.[27] Chemically converted graphene and carbon nanotubes act as a highly selective catalyst for hydroxylation of benzene. But these exciting materials lack high phenol yield.[28] Perfect infinite graphene like sheet lacks efficient defects unlike carbon nitrides where graphitic carbon nitride forms the most stable allotrope of carbon nitrides. Therefore these carbon based 2D sheet like materials have shown to offer support for immobilization of metal or nonmetal catalysts due to its interesting electronic arrangement, facile synthesis, stacked π conjugated planner layer structure and tunable band gap. Selective hydroxylation of benzene molecules have been achieved effectively with modified graphitic carbon nitride namely Cu-Au@g-C_3N_4, Cu-Ag@g-C_3N_4, Fe@g-C_3N_4 and Vanadia@peg-g-C_3N_4 under ambient conditions.[1, 9, 27, 29, 35]

In continuation of our present endeavor in the application of nanocatalysts for synthetically useful organic reactions as well as environmental remediation, we contemplated to develop a simple and energy efficient method for preparation of a novel nanostructured NiO/WO_3@g-C_3N_4. It is also planned to apply this as-synthesized nanostructured NiO/WO_3@g-C_3N_4 material as a visible light driven photocatalyst for oxidation of benzene to phenol and degradation of an antibacterial drug called metronidazole.

Experimental

Materials and physical experiments

Melamine, $Na_2WO_4.2H_2O$, $Ni(NO_3)_2.6H_2O$, benzene and H_2O_2 were purchased from Merck India Ltd. And tert-butanol, ethanol was bought from Sigma-aldrich. Acetonitrile was purchased from Fisher Scientific. All the chemicals were used as they were purchased, without additional purification and double distilled water was used during the course of the experiment. ^{1}H-NMR and ^{13}C-NMR spectra were recorded using a Bruker Advance DPX 300 MHz spectrometer. To evaluate the structure and phase of the photocatalysts, XRD scan was carried through Bruker AXS D8-Advance powder X-ray diffractometer with a scan rate 2° min^{-1} exposed to Cu-Kα radiation (λ=1.5418Å). The surface morphologies were thoroughly analyzed with scanning electron microscopy using JEOL, model JSM-6390LV and the overall morphology was analyzed with transmission electron microscopy using JEOL, model JEM 2100 instrument. UV DRS measurements were carried out using the equipment JASCO UV, Model V-750. XPS patterns were recorded with PHI 5000 Versa Probe II, FEI Inc. Photoluminescence spectra was recorded using Hitachi Model no F-4600 Fluorescence spectrometer. The UV-Visible absorption spectra were measured with UV-Vis double beam spectrophotometer, Model TS2080Plus. Surface area and

View Article Online
DOI: 10.1039/C9NJ02904D

Porosity Measurement (BET) were carried out using 3Flex Version 4.01.

Synthesis of the catalysts

Synthesis of graphitic carbon nitride. Pristine g-C_3N_4 powder was obtained by thermolysis of melamine using a muffle furnace. In the typical method, 5g melamine was heated in a silica crucible with half closed lid at 550°C for 4h at static air condition at a slow ramp. The obtained yellow product was powdered using agate mortar.[35]

Synthesis of Nanostructured NiO/WO_3. NiO/WO_3 heterojunction were synthesized using a novel one step method by dissolving 0.01mol $Na_2WO_4.2H_2O$ in 60ml deionized water and 6ml of tert-butanol followed by slow addition of 0.01mol $Ni(NO_3)_2.6H_2O$ under constant magnetic stirring. After efficient mixing, light blue colored fine precipitate appeared and the mixture was hydrothermally treated in 180°C for 12h using a Teflon lined stainless steel autoclave. The obtained product was then centrifuged under 3000rpm and thoroughly washed with deionized water and ethanol. The product was dried in hot air oven at 60°C.

Synthesis of NiO/WO_3@g-C_3N_4 hybrid. Different ratios of NiO/WO_3@g-C_3N_4 hybrid were prepared by first exfoliating calculated amount of pristine g-C_3N_4 along with NiO/WO_3 nanohybrid in 50 ml deionized water using ultra sonication for 2h. The mixture was stirred overnight and then centrifuged and washed thoroughly and dried in hot air oven at 60°C. According to the percentage of NiO/WO_3, nanohybrids were named as NiWCN-10, NiWCN-15, NiWCN-20, NiWCN-25 and NiWCN-30.

Photocatalytic activity

Hydroxylation of benzene. The photocatalytic performances of the photocatalysts were evaluated by hydroxylation of benzene using H_2O_2 as oxidizing agent in acetonitrile under visible light irradiation with 18 watt household LED light. Before irradiation, the photocatalyst was ultra-sonicated for 10 minutes and reactants were added. To ensure effective mixing, the reaction mixture was magnetically stirred for 30 minutes in dark. The progress of the reaction was assessed using thin film chromatography. The final product was separated and purified using column chromatography and melting point was measured. Again the structure of the organic product was thoroughly investigated with ^1H and ^{13}C NMR spectroscopy.

Degradation of metronidazole

Photocatalytic degradation. Degradation of antibiotic metronidazole in a 20 mgL^{-1} water was also tested using the photocatalysts under sunlight and LED light. Accordingly the photocatalyst was exfoliated with the help of ultra-sonication and after addition of metronidazole the mixture was magnetically stirred for 30 minutes. The progress of the degradation was examined using UV-VIS spectroscopy.

Examination of •OH radical. The involvement of •OH radical in the decomposition was investigated using photoluminescence spectroscopy using benzene-1,4-dicarboxylic acid (terephthalic acid) as probe molecule. Here instead of MZ solution 500ml of 0.5mmol terephthalic acid in 2mmol NaOH solution was irradiated under sunlight. An amount of 4ml of the sample was withdrawn in regular intervals and the formation of 2-hydroxyterephhalic acid was analyzed using PL spectrometer (figure 3d).

Results and Discussion

Pristine g-C_3N_4 powder was obtained by thermolysis of melamine using a muffle furnace and nanostructured NiO/WO_3 was synthesized using a novel one step hydrothermal method. Novel NiO/WO_3@g-C_3N_4 nanohybrid was synthesized using ultra-sonication technique. The synthesis of the heterojunction is represented in scheme 1.

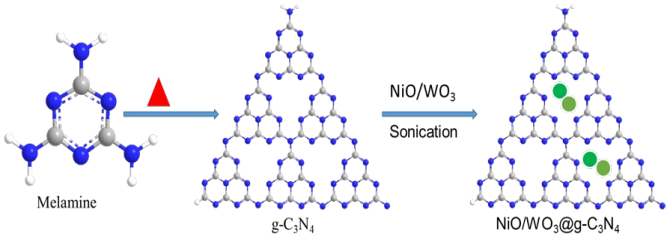

Scheme 1: Schematic representation of synthesis of NiO/WO_3@g-C_3N_4 nanohybrid.

Structure and morphology

The structures of the synthesized photocatalysts was evaluated at 25°C in a continuous scan in the 2θ range 10°-90°. Figure 1 shows the X-Ray Diffraction (XRD) pattern of (a) hydrothermally synthesized NiO/WO_3, (b) g-C_3N_4 and (d) NiO/WO_3@g-C_3N_4. The XRD pattern corresponding for NiO/WO_3 shows peaks at 23.15°, 30.9°, 32.5°, 35.9°, 38.6°, 40.95°, 54.8° and 64.2°, 77.98°, 84.01°,88.18°, 89.05° corresponding to JCPDS file no 47-1049 and 89-4480 for NiO and WO_3 respectively. The XRD pattern for g-C_3N_4 shows peaks at 13.1° and 27.5° corresponding to planes according to JCPDS file no 87-1526. The XRD pattern clearly shows the amorphous nature of the carbon nitride. The XRD pattern of the synthesized nanohybrid shows distinct peaks corresponding to both the component. Figure S1 displayes the XRD patterns of NiO, WO_3, NiO/g-C_3N_4 and WO_3/g-C_3N_4. The X-ray diffraction peaks for NiO and WO_3 corresponds to JCPDS file no 89-5881 and 89-4480 respectively. The XRD patterns of NiO/WO_3, g-C_3N_4 and NiO/WO_3@g-C_3N_4 are plotted in one picture in figure S1 for comparison.

Figure S2 shows the surface morphologies of pure g-C_3N_4, NiO/WO_3 and NiO/WO_3@g-C_3N_4 under a scanning electron microscope (SEM). The surface morphology of g-C_3N_4 clearly displays the two dimensional layered arrangement of extended sheets. The surface also exhibits evident defects which may be

View Article Online
DOI: 10.1039/C9NJ02924B

linked to enhanced catalytic activity figure S2(a). The template free synthesis of NiO/WO_3 nanohybrid leads to irregular morphology comprising predominantly of spheres along with some polyhedron structures figure S2(b). Again the surface of nanohybrid shows co-existence of NiO/WO_3 over 2 dimensional g-C_3N_4 sheets figure S2(c). This also explains the increased surface area and photocatalytic efficiency which is further evaluated with BET analysis The EDX pattern of g-C_3N_4, NiO/WO_3 and NiO/WO_3@g-C_3N_4 gives the elemental weightage of involved photocatalysts thus ensuring the purity of material figure S2(d, e). Furthermore, it also approves the successful synthesis of 25%-NiO/WO_3@g-C_3N_4 nanohybrid.

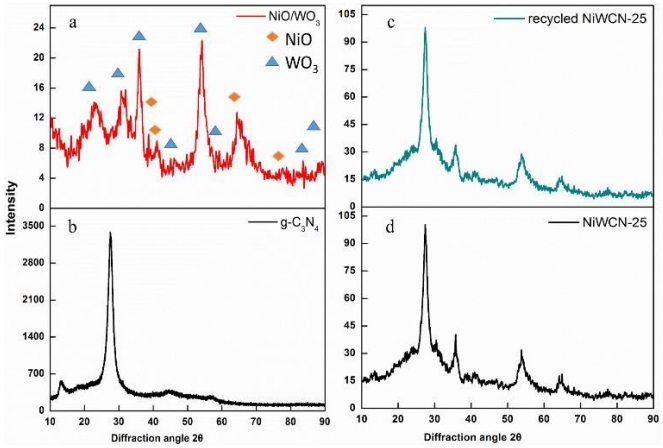

Figure 1: XRD spectra of (a) NiO/WO_3 and (b) g-C_3N_4, (c) recycled NiWCN-25 and (d) fresh NiWCN-25.

The morphology obtained from transmittance electron microscope (TEM) images of synthesized photocatalysts g-C_3N_4 and NiO/WO_3 modified g-C_3N_4 were displayed in the figure S3. The overall morphology of g-C_3N_4 contains two dimensional overlapping lamellar structure. The holes in the two dimensional structure is clearly evident in higher resolution figure S3(b). The modification with NiO/WO_3 enhances irregularity in the structure as NiO/WO_3 nanohybrid is finely dispersed over g- C_3N_4 layers figure S3(c, d). For pure g- C_3N_4 no concentric rings were observed in the SAED pattern figure S3(e). On the other hand distinct concentric rings are observed due to polycrystalinity in case of NiO/WO_3@g-C_3N_4 due to the presence of NiO/WO_3 figure S3(f). The concentric rings corresponds to (1,1,1), (2,0,0) and (2,2,0) planes of cubic NiO and (4,0,2), (42,0), (1,4,2) and (4,2,2) planes of WO_3.

Optical and electronic characterizations

The influence of integration of NiO/WO_3 with g-C_3N_4 in absorption properties are thoroughly studied with the help of UV-Vis Diffuse Reflectance Spectroscopy (UV-DRS) spectroscopy (figure 2). Pristine g-C_3N_4 gives broad absorption centered at 358 nm extending to 500nm. Nanostructured NiO/WO_3 shows very strong absorption peak at 550nm which extends over the complete visible region (figure 2a). Thus modification of g- C_3N_4 with NiO/WO_3 increases absorption in the visible region and shows admirable absorption in the both UV and visible range. The change in band gap of the synthesized photocatalysts was evaluated with the plot of $[\alpha h\nu]^{1/2}$ vs. $h\nu$, as shown in the (figure 2b), here α, $h\nu$ and Eg denotes the absorption coefficient, energy of photon and band gap respectively.[28] The Eg values were found to be 2.74 eV and 2.29 eV for pristine g-C_3N_4 and NiO/WO_3 respectively. Thus incorporation of nanostructured NiO/WO_3 over g- C_3N_4, could increase the production of electron hole pairs by enhanced absorption of visible light, which is beneficial for photocatalytic reactions.

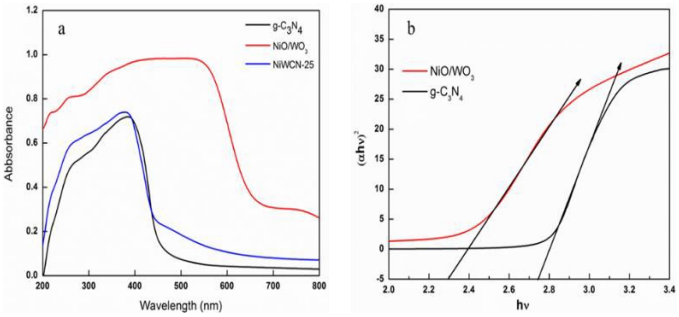

Figure 2. (a) UV-DRS spectra of the synthesized nanomaterials, (b) band gaps of the synthesized nanomaterials.

Photoluminescence (PL) spectra of synthesized nanostructured materials were also analyzed to explain the enhanced photocatalytic performance of NiO/WO_3@g-C_3N_4 (NiWCN-25) than that in pristine g-C_3N_4; as PL properties are directly associated with the separation, transfer and recombination behavior of photogenerated charge carriers and shown in figure 3.[11] The photoluminescence data were recorded for pristine g-C_3N_4 as well as NiWCN-25 with excitation in 370 nm and the PL peaks for both the samples were centered in 443 nm. This clearly illustrates lower recombination probability in the case of NiWCN-25 heterojunction than that in pristine g-C_3N_4 hence better photocatalytic efficiency of NiWCN-25.[31]

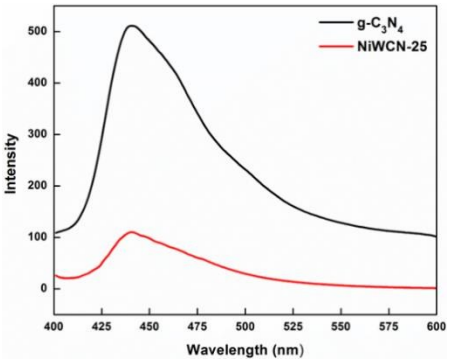

Figure 3: Photoluminescence spectra of g-C_3N_4 and NiWCN-25.

XPS analysis was carried out to explain the oxidation state, binding energy and type of interaction of NiO/WO_3@g-C_3N_4 in addition to the confirmation of material as NiO/WO_3 instead of $NiWO_4$ and shown in figure 4. The full scan XPS survey confirmed the presence of the elements Ni, W, O, C and N in

figure 4(f). The HR-XPS scan of Ni2p is explained in figure 4(d) as having a doublet-split due to Ni-O (which is absent in $NiWO_4$), and Ni-OH bond at 854.1 eV and 856.1 eV respectively. Again a doublet corresponding to Ni-O and Ni-OH interaction located at 871.7 eV and 872.6 eV along with a satellite peak corresponding to $Ni2p_{3/2}$ was observed.[32] Similarly two characteristic peaks centered at 33.8 eV and 35.8 eV for $W4f_{7/2}$ and $W4f_{5/2}$ core binding energies were observed in W4f spectra in figure 4(e).[16] Likewise, two symmetrical peaks were observed in O1s spectra centered at 529.7 eV and 531.6 eV in figure 4(c). For NiO/WO_3 modified g-C_3N_4, the HR-XPS spectrum of C1s displayed two peaks for C-C and N=C=N_2 at 286.6 eV and 283.4 eV in figure 4(a). The XPS spectra of N1s in figure 4(b) displayed asymmetric peak components at 397.2 eV, 399.6 eV and a satellite peak at 402.8 eV. Here the C1s and N1s spectra did not show peaks corresponding to any other covalent interaction other than C and N. These results clearly demonstrate successful formation of NiO/WO_3 modified g-C_3N_4 and the lack of extra peaks for C and N but noncovalent grafting of NiO/WO_3 over g-C_3N_4 surface.

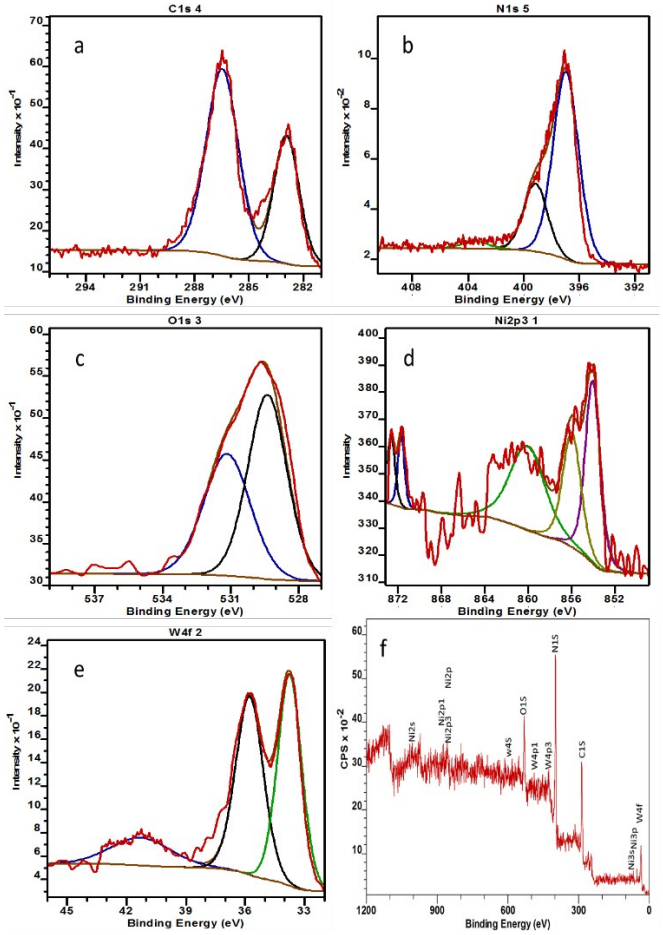

Figure 4: HR-XPS spectrum of involved elements (a) C1s, (b) N1s, (c) O1s, (d) Ni2p and (e) W4f; (f) full scan XPS spectra of NiWCN-25

Surface Analysis. The N_2 adsorption-desorption isotherms for g-C_3N_4 and NiO/WO_3@g-C_3N_4 samples were evaluated in table 1 and figure 5. The nanostructured g-C_3N_4 and NiO/WO_3 modified g-C_3N_4 both have type IV isotherms with narrow H3 type hysteresis loops in the higher relative pressure range, P/P_0, 0.45-1.0 region. Characteristics of capillary condensation in the mesoporous materials with the mesopore of 6.1245nm and 33.2890nm diameter for g-C_3N_4 and NiWCN-25 respectively as analyzed using BJH pore size distribution. The incorporation NiO/WO_3 over pristine g-C_3N_4 surface remarkably increased surface area, pore diameter and pore volume. Thus, the heterostructure offers higher density of catalytically active sites for adsorption of substrates which can be accounted for higher catalytic activity towards hydroxylation of benzene and degradation of metronidazole.

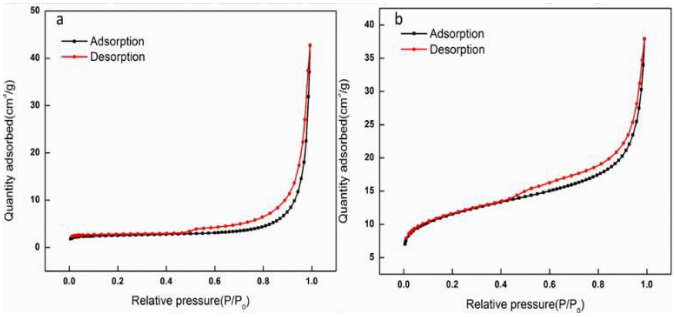

Figure 5: N_2 adsorption-desorption spectra of (a) NiWCN-25 and (b) g-C_3N_4

Table 1. Values for surface area, pore volume and mean pore diameter of the synthesized photocatalysts

SL No	Photocatalyst	Surface area (m^2/g)	Pore volume (cm^3/g)	Mean pore diameter (nm)
1	g-C_3N_4	8.0043	0.059123	6.1245
2	NiO/WO_3@ g-C_3N_4	38.6143	0.166614	33.2890

Hydroxylation of benzene to phenol

Optimization of reaction procedure and reusability test. Initially, the catalytic activities of NiO, WO_3 and g-C_3N_4 were individually tested for hydroxylation of benzene with LED light irradiation using H_2O_2 as oxidizing agent and acetonitrile as solvent room temperature. Activity of g-C_3N_4 was also evaluated at elevated temperature (Table 2, entry 1-4). The catalytic performance of NiO/WO_3 was also tested under same reaction conditions at room temperature and elevated temperature (Table 2, entry 5, 6). NiO and WO_3 individually were interspersed over g-C_3N_4 surface and NiO@g-C_3N_4 and WO_3@g-C_3N_4 were assessed for hydroxylation of benzene in same reaction conditions at room temperature (Table 2, entry 7, 8) and none of these photocatalysts showed admirable results even after 18h of stirring.

Here it was imperative to find that modification of g-C_3N_4 with NiO or WO_3 significantly increase the catalytic activity. Accordingly, different weight percentages of 1:1 NiO/WO_3 were incorporated over pristine g-C_3N_4 surface were synthesized and tested for room temperature visible light aided hydroxylation of

benzene. It is evident from the above table that when 25% of NiO/WO_3 incorporated over g-C_3N_4 best photocatalytic performance was observed (Table 2, entry 9-14). After finding the most active catalyst the reaction conditions were optimized for catalyst amount and it was observed that 50 mg gave the best results. Again the reaction was screened for several solvents; water, methanol, ethanol and acetonitrile. Water and methanol leads to reduction in catalytic efficiency but acetonitrile and ethanol were proved to be perfect solvents for this conversion (Table 2, entry 12, 15-17). The importance of visible light was confirmed with NiWCN-25 catalyst in absence of visible light, the reaction produced low yield and comparatively lower selectivity (Table 2, entry 19). Two blank reactions were also performed in absence of catalyst in optimized conditions in different reaction temperatures and no product was observed (Table 2, entry 20, 21).main paragraph text follows directly on here.

Table 2: Table for catalytic conversion of benzene to phenol

SL No	Catalyst	Time	Temperature	Benzene conversion (%)	Phenol selectivity (%)[a]
1	g-C_3N_4	18 h	RT	--	--
2	g-C_3N_4	18 h	60°C	5	40
3	NiO	18 h	RT	10	55
4	WO_3	18 h	RT	7	42
5	NiO/WO_3	18 h	RT	25	70
6	NiO/WO_3	18 h	60°C	30	73
7	NiO@g-C_3N_4	18 h	RT	45	84
8	WO_3@g-C_3N_4	18 h	RT	32	80
9	NiWCN-10	50 min	RT	40	99
10	NiWCN-15	50 min	RT	52	99
11	NiWCN-20	50 min	RT	65	99
12	NiWCN-25	50 min	RT	85	99
13	NiWCN-25	50 min	60°C	80	99
14	NiWCN-30	50 min	RT	68	99
15	NiWCN-25[b]	50 min	RT	73	81
16	NiWCN-25[c]	50 min	RT	80	85
17	NiWCN-25[d]	50 min	RT	82	96
18	NiWCN-25[e]	50 min	RT	73	99
19	NiWCN-25[f]	18 h	RT	15	80
20	No Catalyst	18 h	RT	--	--
21	No Catalyst	18 h	60°C	--	--

(Reaction condition: The reaction mixture consisted of 2ml benzene and 50 mg catalyst in 10 ml acetonitrile and 4 ml H_2O_2 was added drop wise; [a] The phenol yield was calculated as isolated yield; [b] Solvent water; [c] Solvent methanol; [d] Solvent ethanol; [e] Catalyst recovered after fifth run; [f]. In absence of visible light.

Another series of experiments were conducted to study the recyclability of the photocatalyst NiWCN-25 for transformation of benzene to phenol. After the first cycle was completed, the catalyst was thoroughly separated from the reaction mixture with centrifugation. Then the catalyst was washed thoroughly with water and ethanol and dried at 80°C. The reaction was repeated five times with fresh benzene under optimized reaction conditions, where the catalyst achieved up to 73% of benzene conversion with 99% phenol selectivity (Table 2, entry 18). The recycled photocatalyst was studied using XRD and intensity of peaks due to NiO/WO_3 were seen to be slightly decreased due loss of active catalytic centers (figure 1b). This confirms that NiO/WO_3 has strong non-covalent interactions with g-C_3N_4 which inhibits substantial leaching of active centers.

Plausible Mechanism for Hydroxylation of Benzene. The C-H bond functionalization in hydroxylation of benzene with H_2O_2 as oxidant entails formation of •OH radical from H_2O_2 over photoactive surface of NiO/WO_3@g-C_3N_4. It is postulated that the benzene molecules non-covalently interacts with the NiO/WO_3@g-C_3N_4 surface and gets activated by the heterojunction. Then the photo-generated OH radicals assist the C-H bond activation leading the synthesis of phenol (scheme 2).[1(a), 33]

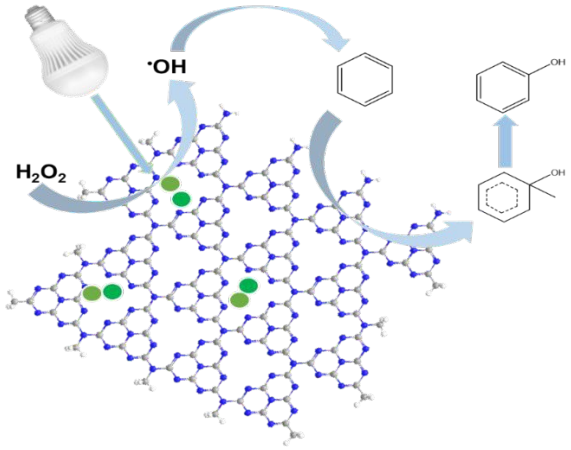

Scheme 2: Plausible mechanism for hydroxylation of benzene

Degradation of Metronidazole

Photocatalytic degradation. A 20 mgL^{-1} aqueous solution of metronidazole was used to evaluate degradation kinetics using g-C_3N_4, NiO/WO_3 and NiWCN-25. A blank reaction was performed in absence catalyst and only 7% degradation of MZ was attained. This inferred the high stability of MZ under solar irradiation. In the optimized processes, 5mg of the catalyst was mixed in 100ml of MZ solution and ultra-sonicated for 5 minutes and then magnetically stirred for 20 minutes in absence of light to ensure physical adsorption equilibrium of MZ on the surface of the catalyst. Then the suspension was irradiated in sunlight.

An amount of 4 ml of the solution is withdrawn at regular intervals, centrifuged immediately and absorbance was measured using a UV-Vis spectrometer. The reaction mixture was continuously stirred to prevent sedimentation of the catalyst. Here the NiWCN-25 catalyst have shown most efficient degradation of the antibiotic metronidazole, as complete degradation was achieved under 90 min, while g-C_3N_4 and NiO/WO_3 attained 15% and 40% degradation (figure 6a, 6b). Another set of reaction was performed with optimized reaction conditions with NiWCN-25 catalyst in LED light irradiation. Here a sluggish reaction rate was recorded as only 73% of MZ was degraded in 90 minutes due to absence of UV light (figure 6b). Again the low photocatalytic decomposition with g-C_3N_4 in solar light was attributed to inadequate energy absorption and fast recombination of photo induced charge carriers. A small increase as compared to g-C_3N_4 in decomposition of MZ was observed with the use of NiO/WO_3 catalyst as it consist a narrower band gap which allows more energy absorption. The mixed phase NiWCN-25 catalyst contains a much higher surface area then g-C_3N_4 and thus offers much more active sites for effective physisorption of MZ along with narrower gap between conduction and valence band than that in g-C_3N_4. Thus with increasing NiO/WO_3 loading over g-C_3N_4 sheets permits more visible light absorption along with slower recombination of photo induced charge carriers due to synergic effects between the two nanostructures. Complete decomposition of MZ was achieved in the shortest time with NiWCN-25 catalyst in comparison to NiWCN-10, NiWCN-15, NiWCN-20 and NiWCN-30. The decreasing photocatalytic degradation of MZ with increase of NiO/WO_3 beyond 25% loading over g-C_3N_4 sheets may be attributed to shielded surface of g-C_3N_4 which hinders effective light absorption.

The improved photocatalytic decomposition of NiWCN-25 catalyst was established using percentage degradation vs. time plot in figure 6(b) and C/C_0 vs. t plot in figure S5(a). The degradation follows first-order kinetics with rate constant 0.0165 min^{-1} shown in figure S5(b). These plots show that the degradation of MZ with NiWCN-25 was more efficient than that with g-C_3N_4, NiO/WO_3 and in absence of catalyst. Here the particularly higher decomposition efficiency of NiWCN-25 catalyst specifies effective synergy between NiO/WO_3 and g-C_3N_4

In order to appraise the involvement of reactive radicals species in the NiO/WO_3@g-C_3N_4 assisted photocatalytic decomposition of MZ, scavengers such as isopropyl alcohol (IA, 10 mmol L^{-1}), 1,4-benzoquinone (BQ, 0.1 mmol L^{-1}) and ammonium oxalate (AO, 6 mmol L^{-1}) were added separately to quench $^{\bullet}OH$, $O_2^{-\bullet}$ and h^+ radicals, respectively (figure 6c).

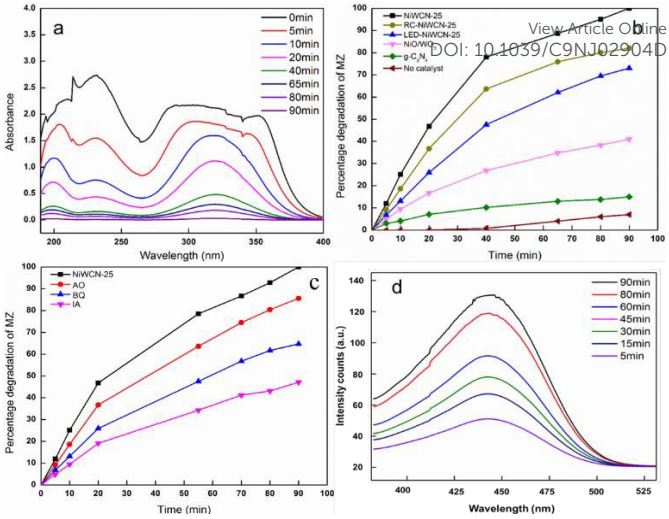

Figure 6. (a) Photodecomposition of Metronidazole with NiWCN-25 over time. (b) Percentage degradation of Metronidazole different catalyst. (c) Percentage degradation of Metronidazole in presence of scavengers IA, AO and BQ. (d) PL spectra observed during irradiation of the NiWCN-25 nanohybrid in a basic solution of terephthalic acid.

Plausible Mechanism for Photocatalytic decomposition of MZ.

Photocatalytic decomposition of organic substrates essentially requires effective involvement of photogenerated charge carriers. The results of the quenching experiments showed sluggish decomposition of MZ (100%, without scavenger) compared to 47.1% (IA), 85.6% (AO) and 64.7% (BQ) which suggest $^{\bullet}OH$, $O_2^{-\bullet}$ and h^+ radicals play pivotal role in the degradation process over NiO/WO_3@g- C_3N_4 (NiWCN-25) surface. Here the addition of IA and BQ incredibly declines the photodegradation process, on the other hand the effect of AO in the degradation process seems comparatively less important and this infers that the $^{\bullet}OH$ and $O_2^{-\bullet}$ were the most important reactive species in the decomposition. The formation of $^{\bullet}OH$ was further confirmed with photoluminescence spectroscopy using terephthalic acid as probe. The visible light absorption of the synthesized heterojunction is significantly enhanced than the carbon nitride as indicated by UV-DRS spectra. Then again the photoluminescence studies of the synthesized materials displayed reduced rate of photogenerated electron hole pairs for NiWCN-25 than in pristine g-C_3N_4. Thus the enhanced visible light absorption, slower recombination of photogenarated charge carriers and confirmed involvement of reactive radical species demonstrates the superior degradation of MZ with NiO/WO_3@g-C_3N_4. Based on these observations a plausible mechanism for photocatalytic decomposition of MZ in presence of sunlight id demonstrated in scheme 3.

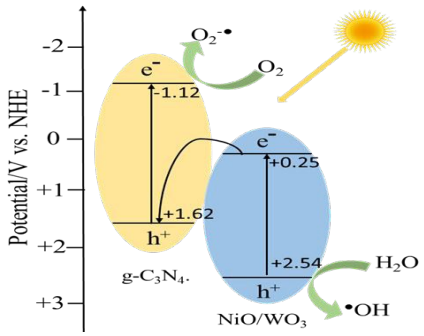

Scheme 3: Plausible mechanism for photocatalytic decomposition of metronidazole.

Conclusions

In summary, a novel nanostructured NiO/WO_3@g-C_3N_4 was prepared by facile and energy efficient method and was investigated as highly efficient reusable heterogeneous photocatalyst for the visible light mediated hydroxylation of benzene with 30% H_2O_2 without involving any toxic reagent. Again a sustainable protocol has been developed for degradation of a potential pharmaceutical pollutant, metronidazole using the NiO/WO_3@g-C_3N_4 photocatalyst under solar irradiation. The involvement of •OH radical metronidazole degradation was also determined using terephthalic acid as probe molecule. The reusability of the photocatalyst was also thoroughly examined and it was found that it can be reused up to five times without observing any appreciable loss in its activity. The graphitic carbon nitride surface not only provide a suitable environment for immobilization of NiO/WO_3 but also absorbs visible light for C-H bond activation in hydroxylation of benzene and degradation of metronidazole.

Conflicts of interest

There are no conflicts to declare.

Acknowledgements

The authors would like to thank the SAIF IIT Kanpur, SAIF Bombay, CSIR-CSMCRI, SAIF Gauhati University, SAIF NEHU and NIT Silchar.

Notes and references

1 (a)S. Verma, R. B. N. Baig and M. N. Nadagouda, *ACS Sustainable Chem. Eng*., 2017, **5**, 3637−3640; b) D. Bianchi, R. Bortolo, R. Tassinari, M. Ricci and R. Vignola, *Angew. Chem. Int. Ed.*, 2000, **39**, 4321-4323; c) X. Chen, J. Zhang, X. Fu, M. Antonietti and X. Wang, *J. Am. Chem. Soc*., 2009, **131**, 11658–11659

2 S. Niwa, M. Eswaramoorthy, J. Nair, A. Raj, N. Itoh, H. Shoji, T. Nimba and F. Mizukami, *Science.*, 2002, **295**, 105-107

3 P. Devaraji, N. K. Sathu and C. S. Gopinath, *ACS Catal*., 2014, **4**, 2844−2853

4 Z. Zheng, B. Huang, X. Qin, X. Zhang, Y. Daib and M. Whangbo, *J. Mater. Chem*., 2011, **21**, 9079–9087 DOI: 10.1039/C9NJ02904D

5 J. W. Han, J. Jung, Y. Lee, W. Nam and S. Fukuzumi, *Chem. Sci*., 2017, **8**, 7119−7125

6 L. Hu, C. Wang, B. Yue, X. Chen and H. He, *RSC Adv*., 2016, **6**, 87656–87664; b) J. Xu, Y. Chen, Y. Hong, H. Zheng, D. Ma, B. Xue and Y. Li, *J. Appl. Catal*., 2018, **549**, 31-39

7 L. Carneiro and A. R. Silva, *Catal. Sci. Technol*., 2016, **6**, 8166-8176

8 P. Borah, A. Datta, K. T. Nguyena and Y. Zhao, *Green Chem*., 2016, **18**, 397-401

9 W. Wang, L. Shi, N. Li and Y. Ma, *RSC Adv.*, 2017, **7**, 12738-12744

10 P. Borah, X. Ma, K. T. Nguyen and Y. Zhao, *Angew. Chem. Int. Ed.*, 2012, **51**, 7756 –7761

11 a) P. Xing, Z. Chen, P. Chen, H. Lin, L. Zhao, Y. Wu, Y. He, *J. Colloid Interf. Sci*., 2019, **552**, 622–632; b) J. Yu, Z. Chen, L. Zeng, Y. Ma, Z. Feng, Y. Wu, H. Lin, L. Zhao, Y. He, *Sol. Energy Mater. Sol. Cells*, 2018, **179**, 45–56 c) J. Y, Z. Chen, Q. Chen, Y. Wang, H. Lin, X. Hu, L. Zhao, Y. He, *Int. J. Hydrogen Energy*, 2018, **43**, 4347-4354; d) P. Chen, P. Xing, Z. Chen, X. Hu, H. Lin, L. Zhao, Y. He, *J. Colloid Interf. Sci*., 2019, **534** ,163−171; e) Z. Chen, P. Chen, P. Xing, X. Hu, H. Lin, L. Zhao, Y. Wu, Y. He, *Fuel,* 2019, **241**, 1−11; f) J. Yu, Z. Chen, Y. Wang, Y. Ma, Z. Feng, H. Lin, Y. Wu, L. Zhao, Y. He, *J. Mater. Sci.,* 2018, **53**, 7453–7465; g) P. Chen, P. Xing, Z. Chen, H. Lin, Y. He, *Int. J. Hydrogen Energy,* 2018, **43**, 19984-19989

12 Y. Morimoto, S. Bunno, N. Fujieda, H. Sugimoto and S. Itoh, *J. Am. Chem. Soc.*, 2015, **108**, 2213−2216

13 X. Cai and B. Xie, *ARKIVOC*, 2015, I, 184-211

14 P. Wu, Z. Liu, D. Chen, M. Zhou and J. Wu, *Appl. Surf. Science*, 2018, **440,** 1101−1106

15 J. Zhang, J. P. Tu, X. H. Xia, Y. Qiao and Y. Lub, *Solar Energy Materials & Solar Cells*, 2009, **93**, 1840−1845

16 G. Cai, P. Darmawan, M. Cui, J. Chen, X. Wang, A. L. Eh, S. Magdassib and P. S. Lee, *Nanoscale*, 2016, **8**, 348-358

17 S. Bulja, R. Kopf, A. Tate and T. Hu, *Scientific Reports*, 2016, **6**, 28839-28843

18 J. Zhang, H. Lu, C, Liu, C, Chen and X. Xin, *RSC Adv*., 2017, **7**, 40499-404509

19 a) L. Niu, Z. Li, Y. Xu, J. Sun, W. Hong, X. Liu, J. Wang and S. Yang, *ACS Appl. Mater. Interfaces*., 2013, **5**, 8044–8052; b) S. Mani, V. Vediyappan, S. Chen, R. Madhu, V. Pitchaimani, J. Chang and S Liu, *Scientific Reports*., 2014, **6**, 24128-24131; c) E. M. Sabolsky, P. Gansor, E. Çiftyurek, K. Sabolsky, C. Xu and J. W. Zondlo, *J. Power Sources*., 2013, **237**, 33-40

20 W. Du, Q. Xu, D. Jin, X. Wang, Y. Shu, L. Kong and X. Hu, *RSC Adv.*, 2018, **8**, 40022-40032

21 W. Ma, B. Yao, W. Zhang, Y. He, Y. Yu, J. Niua and C. Wanga, *Environ. Sci. Nano*, 2018, **5**, 2876-2887

22 a) X. Hu, J. Fan, K. Zhang, N. Yu and J. Wang, *Ind. Eng. Chem. Res*., 2014), 53, 14623−14632

23 a) S. S. Boxi and S. Paria, *RSC Adv*., 2014, **4**, 37752-37760; b) S. S. Boxi and S. Paria, *RSC Adv*., 2015, **5**, 37657–37668

24 a) W. Du, Q. Xu, D. Jin, X. Wang, Y. Shu, L. Kong and X. Hu, RSC Adv. 2018, **8**, 40022- 40034; b) W. Jo and T. S. Natarajan, *ACS Appl. Mater. Interfaces*., 2015, **7**, 17138−17154

25 Y. Yan, T. Ni, J. Du, L. Li, S. Fu, K. Lia and J. Zhou, *Dalton Trans*., 2018, **47**, 6089-6101

26 a) W. Jo, J. Y. Lee and T. S. Natarajan, *Phys. Chem. Chem. Phys*., 2016, **18**, 1000-1016; b) J. Liu, G. Zhang, J. C. Yu and Y. Guoa, *Dalton Trans*., 2013, **42**, 5092-5099

27 W. Ong, L. Tan, Y. H. Ng, S. Yong and S. Chai, *Chem. Rev*., 2016, **116**, 7159−7329

28 a) Q. Wei, H. Fan, F. Qin, Q. Ma and W. Shen, Carbon. 2018, **133**, 6-13; b) W. Shan, S. Li, X. Cai, J. Zhu, Y. Zhou and J. Wang, *ChemCatChem*, 2019, **11**, 1076–1085; c) Y. Zheng, B. Chen, P.

View Article Online
DOI: 10.1039/C9NJ02904D

Ye, K. Feng, W. Wang, Q. Meng, L. Wu and C. Tung, *J. Am. Chem. Soc*., 2016, **48**, 233-237
29 B. Bhuyan, D. J. Koiri, M. Devi and S. S. Dhar, *Mater. Lett*., 2018, **218**, 99–102
30 M. Devi, S. Ganguly, B. Bhuyan, S. S. Dhar and S. Vadivel, *Eur. J. Inorg. Chem.*, 2018, 4819–4825
31 F. T. Li, X. J. Wang, Y. Zhao, J. X. Liu, Y. J. Hao, R. H. Liu and D. S. Zhao, *Appl. Catal. B*., 2014, **144**, 442–453
32 X. Sun, G. Wang, J. Y. Hwang and J. Lian, *J. Mater. Chem.*, 2011, **21**, 16581–16588
33 K. Tian, W. J. Liu, S. Zhang and H. Jiang, *Green Chem*., 2016, **18**, 5643–5650
34 B. Bhuyan, B. Paul, D. D. Purakayastha, S. S. Dhar and S. Behera, *Matt. Lett*., 2016, **168**, 158-162
35 B. Bhuyan, M. Devi, D. Bora, S. S. Dhar and R. Newar, *Eur. J. Inorg. Chem.*, 2018, 3849–3858